Additive Manufacturing 18 (2017) 156–163

Contents lists available at ScienceDirect

Additive Manufacturing

journal homepage: www.elsevier.com/locate/addma

Full Length Article

3D printing electronic components and circuits with conductive thermoplastic filament

Patrick F. Flowers, Christopher Reyes, Shengrong Ye, Myung Jun Kim, Benjamin J. Wiley*

Department of Chemistry, Duke University, 124 Science Drive, Box 90354, Durham, NC 27708, United States

ARTICLE INFO

Article history:
Received 29 April 2017
Received in revised form
13 September 2017
Accepted 1 October 2017
Available online 2 October 2017

Keywords:
Fused filament fabrication
3D printing
Electronics
Conductive filament
Circuits

ABSTRACT

This work examines the use of dual-material fused filament fabrication for 3D printing electronic components and circuits with conductive thermoplastic filaments. The resistivity of traces printed from conductive thermoplastic filaments made with carbon-black, graphene, and copper as conductive fillers was found to be 12, 0.78, and 0.014 Ω cm, respectively, enabling the creation of resistors with values spanning 3 orders of magnitude. The carbon black and graphene filaments were brittle and fractured easily, but the copper-based filament could be bent at least 500 times with little change in its resistance. Impedance measurements made on the thermoplastic filaments demonstrate that the copper-based filament had an impedance similar to a copper PCB trace at frequencies greater than 1 MHz. Dual material 3D printing was used to fabricate a variety of inductors and capacitors with properties that could be predictably tuned by modifying either the geometry of the components, or the materials used to fabricate the components. These resistors, capacitors, and inductors were combined to create a fully 3D printed high-pass filter with properties comparable to its conventional counterparts. The relatively low impedance of the copper-based filament enabled its use for 3D printing of a receiver coil for wireless power transfer. We also demonstrate the ability to embed and connect surface mounted components in 3D printed objects with a low-cost ($1000 in parts), open source dual-material 3D printer. This work thus demonstrates the potential for FFF 3D printing to create complex, three-dimensional circuits composed of either embedded or fully-printed electronic components.

1. Introduction

Printed Electronics has to date generally added value in high-volume production applications where low-cost is critical, and high-performance is not required. Printed electronics have most commonly been made by printing functional inks onto flat surfaces using printing processes usually used in the graphics industry (screen, ink-jet, flexo, gravure, etc.) [1]. Applications for low-cost printed electronics currently include RFID tags, sensors, displays, smartcards, keypads, and packaging [2]. The recent development of tools for additive manufacturing has spurred interest in applying similar techniques to the development of 3D printed electronics. Combining electronically functional materials with the ability of additive manufacturing to create complex 3D geometries from multiple materials can enable the creation of devices that simply are not possible with conventional 2D printing methods designed for the graphics industry, such as multilayer circuit boards, electrical connectors, 3D antennas, mission-specific satellite components, 3D structures with embedded electronics, and batteries [3–6]. Ultimately, the field of 3D printable electronics hopes to enable low-volume, on-site/on-demand production of highly complex and easily customizable electronic structures while reducing material waste, energy consumption, prototyping time, and cost relative to conventional electronics fabrication methods [2].

Current approaches to 3D printing electronics generally fall into one or more of the following categories: (1) surface direct write, (2) post-processing by injection or electroplating, (3) freeform 3D printing [2,7]. The surface direct write technique involves printing on a 3D surface rather than printing free-standing 3D structures. Processes that fall into this category include droplet-based (Ink-jet, Aerosol Jet™) [3,8–11], laser-based [12,13], and extrusion-based methods [14–17]. The strengths and weaknesses of these various techniques have been described in depth elsewhere [2,18]. Interest in 3D printed electronics has motivated the development of several new commercially available equipment that use these different processes. For example, Nano Dimesion's DragonFly 2020 (available for ~$50 k and released in 2016) enables multilayer printing of conductive traces using an inkjet technique at a lateral resolu-

* Corresponding author.
E-mail address: bjw24@duke.edu (B.J. Wiley).

https://doi.org/10.1016/j.addma.2017.10.002
2214-8604/

tion of ~30 μm [19]. Currently this printer utilizes proprietary Ag and dielectric nanoparticle inks. In general, it can be very difficult and time consuming to develop novel electronic inks for ink-jet processes due to the need to tune the surface tension and viscosity (8–12 cp) of the ink to obtain a desired droplet size (~30 μm) and reproducible jetting characteristics. In addition, clogging can be an issue if the size of the particles or amount of solids in the ink is too high. The Aerosol Jet™ process, developed by Optomec, circumvents many of these issues by enabling the printing of smaller droplets (1–5 μm) from inks with a wider range of viscosities (1–1000 cp) [20]. The Aerosol Jet™ (available since 2004) uses a sheath gas as the nozzle, thereby eliminating many of the clogging issues that plague ink-jet, and enabling the use of a much wider variety of materials in the inks. However, the cost of Aerosol Jet™ systems ranges from $295 k to $495 k, making them out of reach for many potential users. In comparison, the Voxel8 (released in 2016), which combines a conventional plastic filament extrusion nozzle with a syringe-based silver ink extruder, is less expensive at $9k for the developer kit [21]. The lateral resolution of the traces that can be printed with the Voxel8 is 250 μm with a recommended pitch of 2 mm [22], and the printer allows pausing of the print to enable manual placement of circuit components. However, as with ink-jet and Aerosol Jet™, the Voxel8 has a limited capability to print freestanding structures in the z-direction, with recommended trace thicknesses <500 μm.

To circumvent the high-cost and limitations of dedicated 3D printed electronic systems using surface direct write processes, there have been efforts to develop post-processing techniques for 3D printed parts to imbue them with the desired electronic properties. Perhaps the most popular of these is electroplating a plastic part, which can be accomplished after an initial metallization with electroless deposition or conductive paint. Swissto12 has used this technique to produce a variety of 3D printed antennas and waveguides, and Yurduseven et al. demonstrated metallization of 3D printed cavity antennas for imaging [23,24]. However, this technique produces chemical waste and it can be difficult to achieve consistent, high-quality results. Wu et al. showed that 3D conductive traces could be created by injecting silver paste into 3D printed channels, and used this process to create passive wireless sensors. However, the filling process had to be repeated five times to fill ~70% of the channel with paste, and the smallest channel that could be filled was 600 μm.

Freeform 3D printing can make three-dimensional electronic structures, without the requirements of an existing 3D surface or post-processing. For example, syringe-based printing of sheer-thinning silver nanoparticle inks was used to make freestanding, three-dimensional interconnects [17]. However, these inks required sintering at high temperatures (~250 °C) to become conductive in 30 min. Ladd et al. demonstrated that gallium liquid metal alloys can be extruded from a nozzle to form freestanding, out-of-plane metal structures up to a few millimeters in height that are stabilized by the material's oxide shell [25]. The liquid metal does not require sintering, and can be embedded in PDMS to create stretchable devices, but its liquid nature means that the freestanding structures cannot be used for practical applications. In principle, either sheer-thinning inks or liquid metals can be printed with low-cost (<$200), fused filament fabrication (FFF) 3D printers by replacing the original polymer extruder with a syringe-based extruder consisting of 3D printed parts [26].

In terms of low-cost, accessibility, and ease of use, it would be ideal to create a highly conductive polymer filament that can be used directly with FFF printers to create electronic components and interconnects without the requirement of sintering, electroplating, or any other post-processing. This would allow many people who already own a 3D printer to create their own custom 3D printed electronics. Until recently, however, the only conductive materials that were commercially available for FFF printers were two carbon-based filaments, Black Magic 3D and Proto-pasta, which have a reported volume resistivity of 0.6 Ω cm and 30 Ω cm, respectively. Researchers have shown that similar materials can be used to create resistive flex and touch sensors [27], but these high resistivities are not suitable for use as conductive traces. For example, a 10-cm-long, 2-mm-thick trace made from Black Magic 3D and Proto-pasta would be 150 Ω and 7500 Ω, respectively. Thus, these materials are better suited for printing of resistors rather than interconnects.

Given our lab's previous experience with highly conductive, copper-based nanostructures [28,29], we decided to create a conductive filament that could be used to print electronic components and interconnects with low-cost, FFF-based 3D printers. The resulting copper-based filament, Electrifi, has a resistivity of 0.006 Ω cm and is commercially available [7]. Further details as to how to make a filament with this level of resistivity will be reported elsewhere. Recent reports have demonstrated applications of Electrifi at microwave frequencies, demonstrating the material can be used to 3D print microstrip transmission lines, frequency-diverse metasurface antennas and 3D metamaterial building blocks [30–32]. In this article, we use a combination of commercially available dielectric and conductive filaments to demonstrate the potential for additive manufacturing of basic electronic components and circuits with low-cost FFF technology. Conductive traces, resistors, capacitors and inductors were printed with both single and dual-extrusion. The high conductivity of Electrifi allows for 3D printing of AC radio frequency (RF) circuits, a wireless power transfer circuit, and a high-pass filter. We show Electrifi can be used in conjunction with a dual-material printer to electrically connect standard surface mount components, such as an LED, by printing over the pads of a component embedded in 3D printed plastic. Finally, we demonstrate that Electrifi can be used to 3D print flexible conductive traces, multi-level embedded conductive traces, as well as freestanding, thin-walled structures such as a horn antenna.

2. Methods

2.1. Materials

Hatchbox PLA and ColorFabb bronze-fill PLA were used as dielectric materials. Electrifi (Multi3D LLC), a graphene-based conductive PLA (Black Magic 3D), and a carbon black-based conductive PLA (Proto-pasta) were used as conductive materials. BuildTak and painter's tape were used as build surfaces.

2.2. Fabrication

The prevention of cross contamination during dual-extrusion, i.e., the mixing of two filament materials during printing, is critical to printing electronic components because cross contamination of the conductive material will result in either shorting between conductive traces, or in the interruption of a conductive trace with non-conductive material. Although many printers are available with multiple nozzles, all printers we have tested (Prusa i3, Hictop, CTC 3D, and LulzBot Taz 5) are not able to prevent cross-contamination. Typical multimaterial printers use two separate nozzles at the same z height, but this method leaves the inactive nozzle in a position where it is likely to scrape across the printed surface and cause cross-contamination.

One approach that has been advertised as a way around this issue is to extrude multiple materials through the same nozzle. To change the printed materials with a single extruder, the old filament is programed to retract all the way out of the hotend and a new filament is then fed into the hotend by a separate stepper motor. However, the old material must be cleared out of the noz-

Table 1
Printing Parameters.

Material	Extrusion Temp (°C)	Print Speed (mm/s)	Extrusion Multiplier
PLA	185–190	30–40	0.9–1.05
Bronze-fill	195	20	1.1
Proto pasta	190	40	1.0
Black Magic	190	40	1.0
Electrifi	140	15	1.15

zle by purging 40 mm or more of filament through it, resulting in a significant amount of waste and added cost for a part that requires material changes in every layer. In addition, if the two filaments require different printing temperatures, the nozzle will likely clog.

Due to the limitation of suitable commercially available printers for dual-material printing, we chose to build our own 3D printer. The design of our printer is based off the open source D-Bot printer [33], and has a total parts cost under $1000 (Fig. S1A Supporting Information). The original design, which is described by a detailed build guide and bill of materials, was converted from single to dual extrusion, and the Bowden extruder was changed to direct drive. A Bowden extruder pushes filament through a long tube before it reaches the nozzle, which frequently results in softer filaments bending and getting jammed inside the tube due to the back pressure from the nozzle. A direct drive system, in which the extrusion motor sits directly above the nozzle, pushes on a shorter piece of filament so that bending and jamming occurs less frequently. A dual-direct drive system has enough weight to bend the 8-mm-rods typically used in low-cost 3D printers up to ~200 μm, but the aluminum extrusions used in the D-Bot printer can easily accommodate the increased mass. To address the cross-contamination problem, we incorporated Dglass3D's Autolift retractable hotends (Fig. S1B Supporting Information). These hotends have integrated bushings which cause the nozzles to retract when the filament is not extruded through the nozzle.

Fusion360 was used to create 3D models of components, which were then imported to Simplify 3D slicing software to generate 3D printable gcode files. 3D models of the objects printed here have been made available online [34]. The printing parameters used for each filament are listed in Table 1. When printing separator material for the capacitor, PLA and Bronze-fill were over-extruded slightly to ensure each separator layer was completely solid and would not short. Another important note is the thermal expansion of Electrifi is significantly different from PLA and it thus requires a higher extrusion multiplier to print solid traces. No heated bed was used on any of these prints to preserve the conductive properties of Electrifi. Instead, items were printed on BuildTak and painter's tape surfaces at room temperature.

2.3. Characterization

DC IV curves for conductive traces were measured with a Keithley 2400 SourceMeter. Resistance Measurements for resistors were taken with a Fluke Multimeter. Electrochemical Impedance Spectroscopy (EIS) was performed with a BioLogic SP-200 to determine capacitance and inductance for the capacitor and inductor components, respectively. The data were fit to an equivalent circuit model to obtain capacitance and inductance values. A Hantek DSO-5200A oscilloscope was used to analyze the wireless power transfer capabilities of the inductor. A Gratten ATF20B function generator in combination with the Hantek oscilloscope was used to characterize the high-pass filter demo circuit. Silver paste from Electron Microscopy Sciences was applied to the contact pads/screw terminals of each sample and allowed to dry for at least 24 h before testing to minimize contact resistance from the test leads.

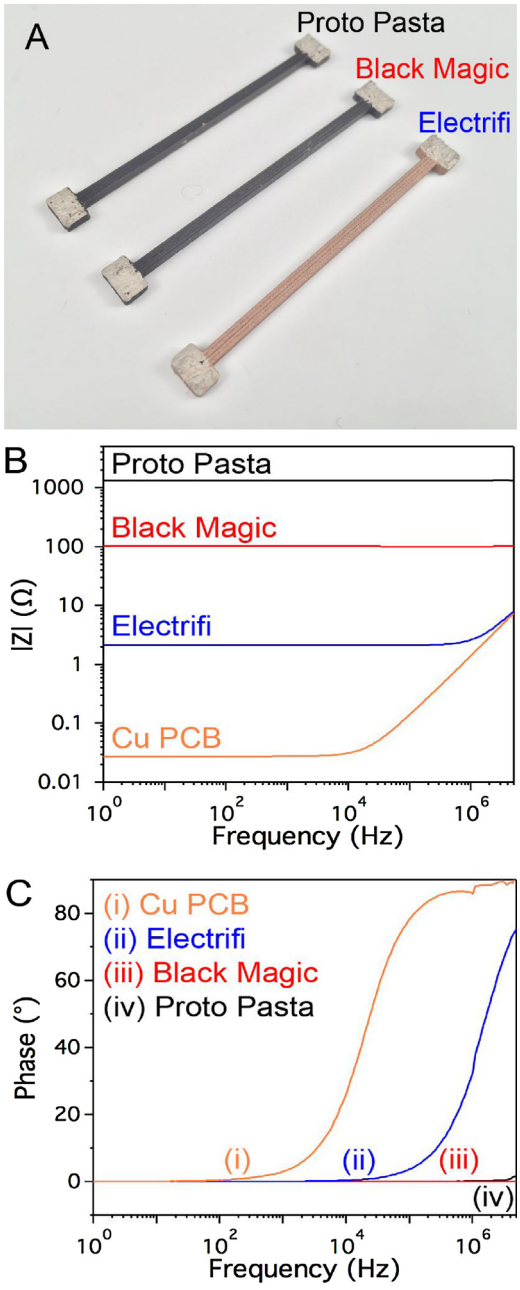

Fig. 1. (A). 2 × 2 × 50 mm traces of Electrifi, Black Magic, and Proto pasta filaments were printed to test their viability for use as conductive traces in a circuit. Electrochemical Impedance Spectroscopy was then performed over the frequency range 1 Hz–5 MHz on each material to discover their (B) impedance and (C) phase behavior. The impedance and phase of a 1 oz Cu PCB trace of the same length and width was also measured (orange line) for comparison. (For interpretation of the references to colour in this figure legend, the reader is referred to the web version of this article.)

3. Results and discussion

Three of the most central and basic electronic components are resistors, capacitors and inductors. By combining these three basic components, a wide range of electronic circuits can be fabricated including voltage/current dividers, sensors, oscillators, relays, crossovers, transformers and filters [35]. Of course, to electrically connect these components one also needs a conductor, which should ideally contribute a negligible amount of resistance to an electrical circuit. This is often taken for granted in the design of electronic circuits wherein highly conductive (~2×10^{-6} Ω cm)

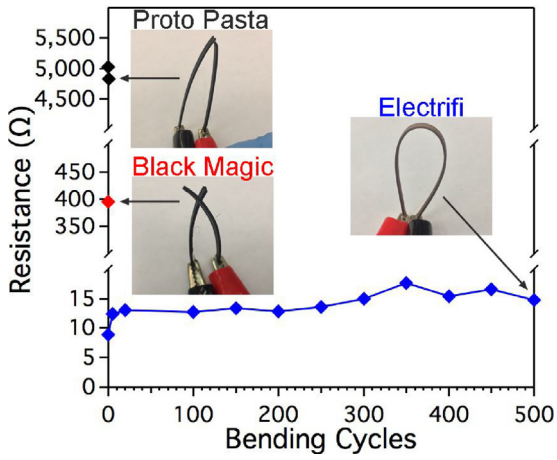

Fig. 2. Bending test on 100 mm long × 2 mm wide × 1 mm high conductive traces. The printed traces were repeatedly bent in half 180° and resistance measurements were taken periodically in the unbent orientation. Black Magic snapped on the first bend, while Proto pasta snapped on the second bend. Electrifi was bent 500 times without snapping.

copper traces are commonplace, but the relatively high resistivity of 3D printed traces requires that one take their non-negligible resistance into account.

3.1. Conductor

Fig. 1A shows printed traces of commercially available conductive materials measuring 2 × 2 × 50 mm. The impedance magnitude (|Z|) and phase behavior of each trace was measured over a range of frequencies from 1 Hz to 5 MHz (Fig. 1B and C). A single-sided, 1 oz (35 μm thick) Cu PCB trace of identical length and width was also tested for comparison. The impedance of the Cu PCB trace increases at 10 kHz due to the contribution of inductive reactance, but resistance of the carbon-based materials is so large that minimal inductive reactance was observed over the range of frequencies tested. In contrast, inductive reactance was observed in the Electrifi trace, but its contribution began at a frequency 100× higher (100 kHz) than the Cu PCB trace. Interestingly, the impedance of the Cu PCB trace is roughly equivalent to the Electrifi impedance at 1 MHz.

The flexibility of the conductive materials was also investigated by bending 100 mm long, 2 mm wide, and 1 mm thick traces in half (Fig. 2 inset). Black Magic could not complete 1 bend cycle before fracturing while Proto pasta fractured on the second bend. Electrifi, on the other hand, was bent 180° for 500 cycles (Fig. 2 inset). The results show that the resistance approximately doubles during the first few cycles, but the resistance stabilizes thereafter. The greater flexibility of Electrifi is likely due to the fact that it is made from a more flexible biodegrable polyester rather than the PLA used in the carbon-based filaments.

3.2. Resistor

When a resistive element is desired in a 3D printed circuit it is necessary to achieve predictable, and reproducible resistance values. This can be achieved by altering the dimensions of the resistive element and the material from which it is made. Fig. 3A shows that by simply varying the cross-sectional area of 50 mm long printed traces, resistors with values ranging from 10 Ω to 10 KΩ can be obtained. Fig. 3B shows a linear trend can be obtained from these results which follows Ohms law (Eq. (1)):

$$R = \rho \frac{L}{A} \tag{1}$$

where R is the resistance, L is the length of the trace, ρ is the resistivity of the trace material, and A is cross-sectional area of the trace. From these linear fits we determined the resistivities of the printed filaments to be 12, 0.78, and 0.014 Ω cm for Proto pasta, Black Magic, and Electrifi, respectively. Not only do these three materials enable one to 3D print resistors with a wide range of commonly used values, they allow one to customize the resistance to best fit a desired application.

3.3. Inductor

Given that the carbon-based filaments are not sufficiently conductive to serve as inductors, we focused on using Electrifi to print several air-core spiral inductors. This type of inductor is commonly used in RF electronic circuitry. Three different inductors were fabricated with different numbers of turns (5–9). Dual printing was necessary to fabricate these structures as the innermost coil of a spiral inductor must bridge over or under the inductor to connect to the rest of an electrical circuit as shown in Fig. 4A. We used PLA as an insulating dielectric material in our structures. EIS data was fit to an $L_1 + R_1$ equivalent circuit model to obtain inductance values (Fig. 4B solid line). Wheeler's approximation (Eq. (2)) was used to calculate the predicted inductance for these geometries,

$$L = \frac{r^2 n^2}{8r + 11w} \tag{2}$$

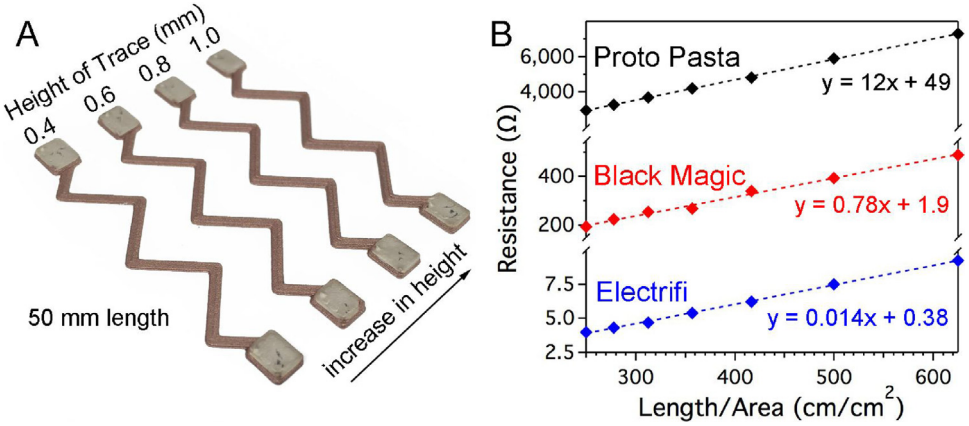

Fig. 3. (A) Thin 0.5 mm wide, 50 mm long traces with varying heights were printed using Electrifi (shown), Black Magic and Proto pasta. (B) The resistance of each trace was measured using a multimeter and their resistance as a function of inversed cross sectional area was plotted showing a good linear relationship for each.

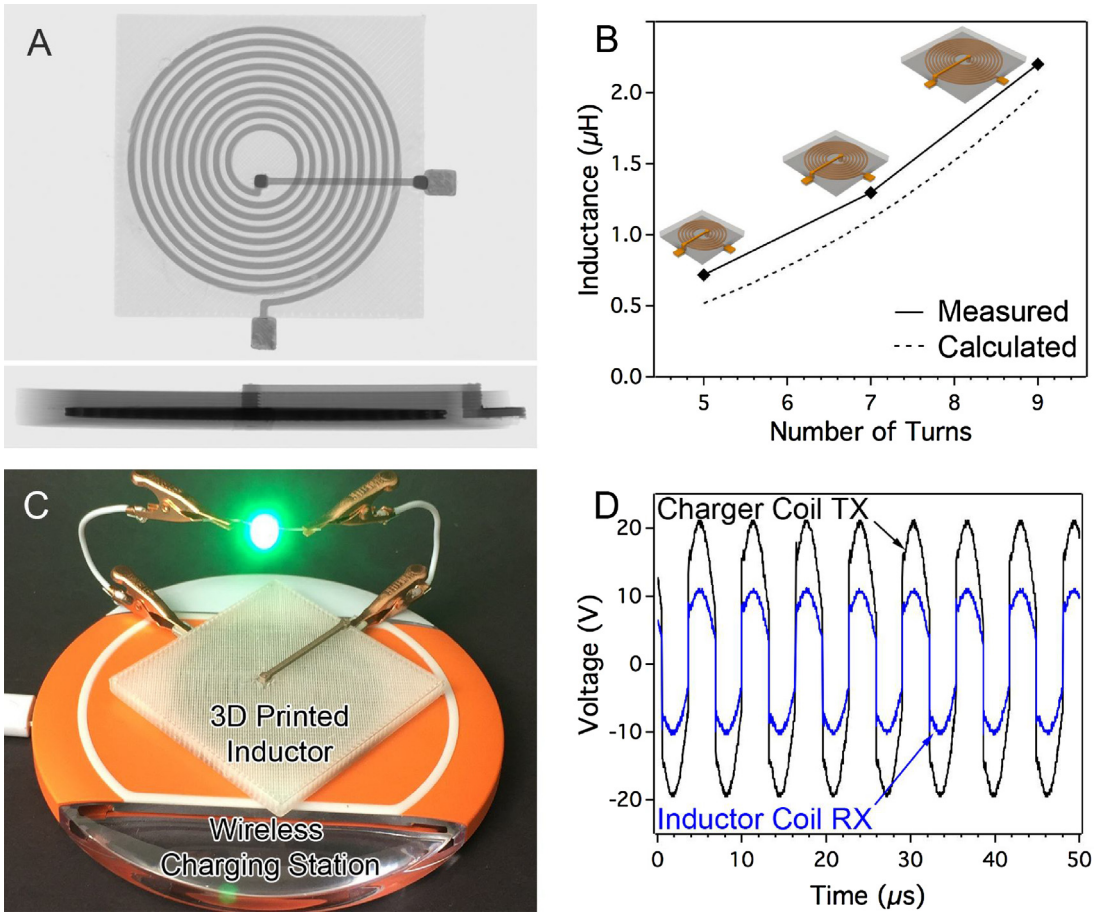

Fig. 4. (A) Micro CT image of 3D printed spiral inductor in top-view and side-view. (B) Inductance as a function of number of turns. (C) Demonstration of wireless power reception using the 9 turn spiral inductor. (D) Oscilloscope measurement of the transmitted and received waveforms.

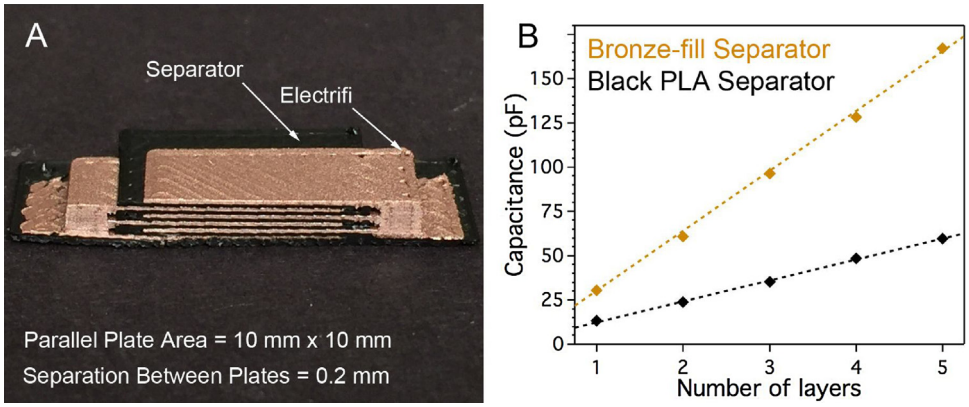

Fig. 5. (A) Half-slice view of the printed five-layer parallel plate capacitor with black PLA separator. (B) Plot of capacitance versus the number of stacked parallel plate layers for two different separator materials.

where L is inductance in μH, r is the mean radius of the inner and outer edges of the spiral in inches, n is the number of turns, and w is the width of the coil in inches [36]. The equation was applied to our printed inductor geometries and plotted for comparison to the measured inductances (Fig. 4B dotted line). A good correlation is evident despite a systematic error of 0.2 μH in the measurements. The parameters used in this calculation are included in Supporting Information Table S1.

As a simple demonstration of the ability of the coil to receive wireless power, a commercial wireless phone charger was used to power an LED connected to a 9-turn 3D inductor (Fig. 4C). Fig. 4D shows the transmitted and received waveforms during the wireless power transfer process. This inductor also demonstrates the ability of dual-material FFF printing to create multilevel conductive traces which can cross over one another, thereby opening up the possibility to create much more complicated electronic circuits that would not be possible if limited to a single printed layer.

3.4. Capacitor

Parallel plate capacitors were 3D printed using Electrifi as the conductive material, and two types of PLA, Black-pigmented and

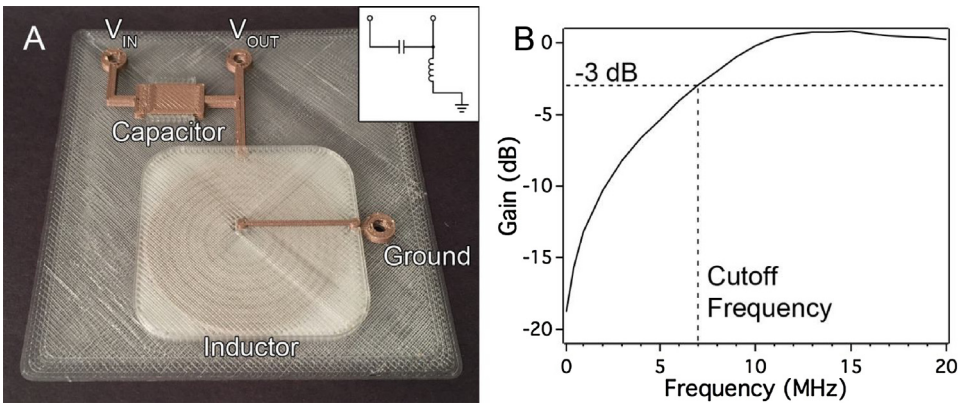

Fig. 6. (A) Fully 3D printed high-pass filter LC circuit. (B) Measured filtering characteristics for the functional high-pass circuit.

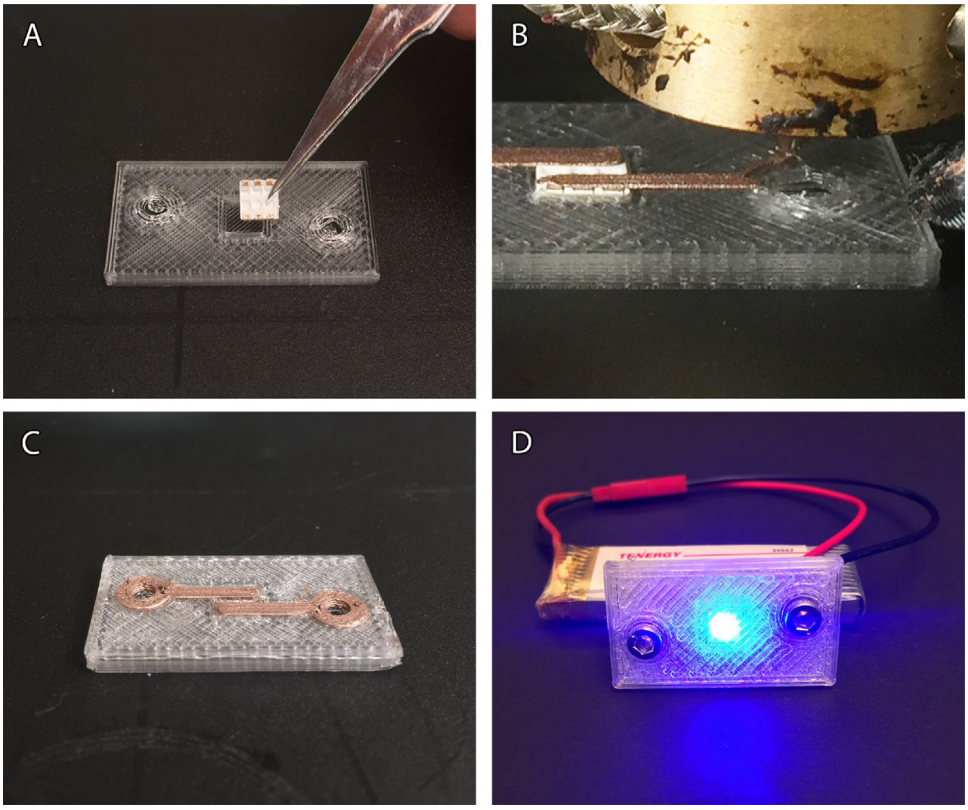

Fig. 7. Embedded LED as an example of interfacing with off-the-shelf components. (A) Printing process is paused and LED is placed into a cavity before resuming the print. (B) Conductive traces are printed on top of the LED contacts, and (C) the LED component is fully embedded. (D) Screw terminals are used to attach a battery to the Electrifi traces and light the LED.

bronze particle-filled, as the dielectric. The overlapping dimensions of the parallel plates is 10 mm × 10 mm with a vertical separation distance of 0.2 mm (Fig. 5A). Eq. (3) shows that for a parallel plate capacitor the magnitude of capacitance can be easily tuned by altering 4 parameters:

$$C = n\frac{k\varepsilon_0 A}{d} \tag{3}$$

where k is the relative dielectric permittivity of the separator, ε_0 is the vacuum permittivity, A is the overlapping area of the conductive plates, d is the separation distance between plates, and n is the number of stacked capacitors. Relative permittivity can be altered by changing the separator material, and the geometry (A, d, and n) can be varied to achieve a desired capacitance value.

Fig. 5B shows the capacitance values obtained from a $C_1 + R_1$ equivalent circuit fit of an EIS measurement on printed capacitors with values of n between 1 and 5. The capacitance scaled linearly with the number of stacked layers for capacitors made with either black PLA or Bronze-fill PLA. Using the measured capacitance and Eq. (3), we calculated the dielectric constant k of (black) PLA to be 2.66, which is in good agreement with literature values ranging from 2.4 to 2.8 [37,38]. As expected, bronze-filled PLA exhibited higher capacitance values because the incorporation of an oxide-coated metal particle filler increases the dielectric constant [39]. The dielectric constant of the bronze-filled PLA was 7.35.

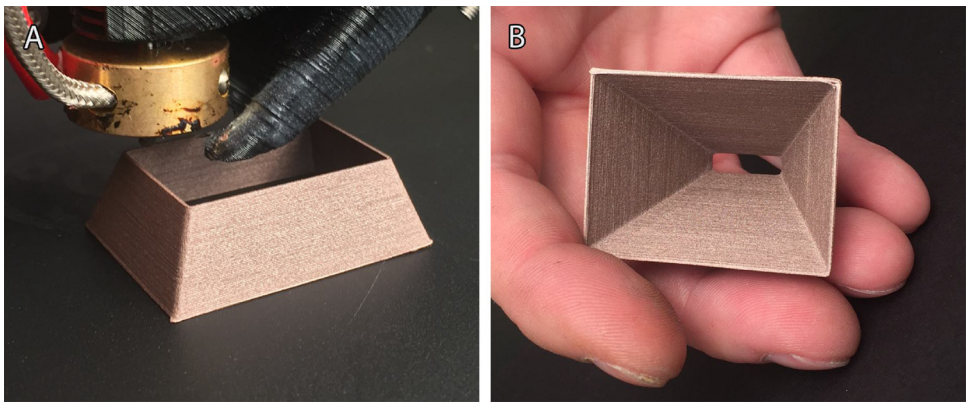

Fig. 8. (A) Printing of a thin-walled hollow pyramid structure which could be used as a horn antenna. No supports were used. (B) The completed structure is 0.5 mm thick, 30 mm tall, with 55° angled walls.

3.5. High-pass filter

To evaluate the performance of these 3D printed components in a functional circuit, a high-pass filter was designed and printed using dual printing. High-pass filters are commonly included in AC circuits whenever lower frequencies may cause signal interference. The fully 3D printed filter circuit consists of a 60 pF capacitor, a 2.2 μH inductor, conductive traces, PLA dielectric, and screw terminal breakouts (Fig. 6A). A sinusoidal waveform was applied to the input of the circuit and the output waveform was measured. The results showed that low frequencies were successfully filtered out with a cutoff frequency at approximately 7 MHz (Fig. 6B). The cutoff frequency is defined as the frequency at which 50% of the input signal is filtered, causing it to drop by −3 dB. The signal is filtered by ∼20 dB per decade which is comparable to the performance of a conventional first-order passive high-pass filter [40].

3.6. Embedded component

Similar to the chip insertion capability demonstrated by the Voxel8, we can use the open-source 3D printer to pause a print, insert a component, and print Electrifi over the contact pads of the component to complete the circuit. To demonstrate this capability, a 3D model was first designed which included a cavity in the shape of the package for a 5050 LED. The model was then printed and the printing process was interrupted at the top of the cavity. The 5050 LED was then manually placed into the cavity as shown in Fig. 7A. After the print is resumed, conductive traces are printed over the top of the LED contacts (Fig. 7B). Screw terminals were used to connect a battery to the circuit (Fig. 7C), and the brightly lit LED is shown in Fig. 7D. This simple example demonstrates that when the use of conventional electronic components is desired or required, they can easily be integrated into 3D objects using FFF printing.

3.7. Freestanding conductive structures

A distinct advantage conductive thermoplastics have over conductive inks and pastes is the ability to create large unsupported 3D structures. Fig. 8A and B demonstrate how this capability can be exploited to fabricate useful conductive 3D structures. Here a hollow pyramid structure with 0.5 mm thick, 35 mm tall walls at 70° angles printed with Electrifi. Such structures are often used in radio frequency (RF) applications as horn antennas.

4. Conclusions

This paper demonstrates the viability of using FFF 3D printing to fabricate many commonly used electronic components individually, as well as printing complete circuits comprised of multiple components in one step. These results are a first step towards the goal of establishing a library of 3D printed electronic elements with detailed designs, printing conditions, and expected properties. The versatility of FFF to create conductive features in three dimensions is demonstrated in the printing of a capacitor, inductor, and high-pass filter. We hope that these examples will catalyze the expansion of FFF 3D printed electronics as much work remains to be done in designing components and printing methods that take advantage of the new materials that are being developed for FFF printing.

Acknowledgements

This work was supported by an NSF CAREER award (Grant DMR-1253534) and NSF Grant No. ECCS-1344745. Patrick Flowers would like to acknowledge David Spaulding for sharing the design for his printer and his advice during the initial build. Patrick Flowers would also like to thank Professor David Norwood for the insightful discussions on inductor theory.

Appendix A. Supplementary data

Supplementary data associated with this article can be found, in the online version, at https://doi.org/10.1016/j.addma.2017.10.002.

References

[1] R.N. Das, H.T. Lin, J.M. Lauffer, V.R. Markovich, Printable electronics: towards materials development and device fabrication, Circuit World 37 (2011) 38–45.
[2] D.P. Parekh, D. Cormier, M.D. Dickey, Multifunctional printing incorporating electronics into 3D parts made by additive manufacturing, in: Amit Bandyopadhyay, Susmita Bose (Eds.), Additive Manufacturing, CRC Press, 2015, pp. 215–258.
[3] K.K. Christenson, J.A. Paulsen, M.J. Renn, Direct printing of circuit boards using Aerosol Jet®, NIP Digit. Fabric. (2011) 433–436.
[4] E. MacDonald, R. Wicker, Multiprocess 3D printing for increasing component functionality, Science 353 (2016) aaf2093.
[5] D. Espalin, D.W. Muse, E. MacDonald, R.B. Wicker, 3D printing multifunctionality: structures with electronics, Int. J. Adv. Manuf. Technol. 72 (2014) 963–978.
[6] C. Shemelya, L. Banuelos-Chacon, A. Melendez, C. Kief, R. Wicker, G. Krijnen, et al., Multi-functional 3D printed and embedded sensors for satellite qualification structures, Sensors (Basel) (2015) 1422–1425.
[7] Electrifi Conductive 3D Printing Filament, Multi3d, 2016, http://www.multi3dllc.com (Accessed 9 March 2017).

[8] B.K. Park, D. Kim, S. Jeong, J. Moon, J.S. Kim, Direct writing of copper conductive patterns by ink-jet printing, Thin Solid Films 515 (2007) 7706–7711.
[9] K. Woo, D. Kim, J.S. Kim, S. Lim, J. Moon, Ink-jet printing of cu-ag-based highly conductive tracks on a transparent substrate, Langmuir 25 (2009) 429–433.
[10] B.J. de Gans, P.C. Duineveld, U.S. Schubert, Inkjet printing of polymers: state of the art and future developments, Adv. Mater. 16 (2004) 203–213.
[11] M.J. Catenacci, P.F. Flowers, C. Cao, J.B. Andrews, A.D. Franklin, B.J. Wiley, Fully printed memristors from Cu–SiO2 core–shell nanowire composites, J. Electron. Mater. 46 (2017) 4596–4603.
[12] C.B. Arnold, P. Serra, A. Piqué, Laser direct-write techniques for printing of complex materials, MRS Bull. (2007).
[13] D.B. Chrisey, A. Piqué, R. Modi, H.D. Wu, R.C.Y. Auyeung, H.D. Young, Direct writing of conformal mesoscopic electronic devices by MAPLE DW, Appl. Surf. Sci. 168 (2000) 345–352.
[14] Y. Jo, J.Y. Kim, S.-Y. Kim, Y.-H. Seo, K.-S. Jang, S.Y. Lee, et al., 3D-printable, highly conductive hybrid composites employing chemically-reinforced, complex dimensional fillers and thermoplastic triblock copolymers, Nanoscale 11 (2017) 4237.
[15] J.J. Adams, E.B. Duoss, T.F. Malkowski, M.J. Motala, B.Y. Ahn, R.G. Nuzzo, et al., Conformal printing of electrically small antennas on three-dimensional surfaces, Adv. Mater. 23 (2011) 1335–1340.
[16] M. Mirzaee, S. Noghanian, L. Wiest, I. Chang, Developing flexible 3D printed antenna using conductive ABS materials, 2015 IEEE International Symposium on Antennas and Propagation & USNC/URSI National Radio Science Meeting, IEEE (2015) 1308–1309.
[17] B.Y. Ahn, E.B. Duoss, M.J. Motala, X. Guo, S.-I. Park, Y. Xiong, et al., Omnidirectional printing of flexible, stretchable, and spanning silver microelectrodes, Science 323 (2009) 1590–1593.
[18] R.L. Truby, J.A. Lewis, Printing soft matter in three dimensions, Nature 540 (2016) 371–378.
[19] Nano Dimension, http://www.nano-di.com (Accessed 16 April 2017).
[20] Optomec, https://www.optomec.com/ (Accessed 28 March 2017).
[21] Voxel8, http://www.voxel8.com (Accessed 9 March 2017).
[22] Design Guidelines, Voxel8, http://support.voxel8.co/hc/en-us/articles/207448823-Design-Guidelines (Accessed 16 April 2017).
[23] O. Yurduseven, J.N. Gollub, D.L. Marks, D.R. Smith, Metallization of a 3D printed cavitiy for imaging, 2016 IEEE International Symposium on Antennas and Propagation & USNC/URSI National Radio Science Meeting, IEEE (2016) 855–856.
[24] Swissto12, http://www.swissto12.com (Accessed 8 April 2017).
[25] C. Ladd, J.-H. So, J. Muth, M.D. Dickey, 3D printing of free standing liquid metal microstructures, Adv. Mater. 25 (2013) 5081–5085.
[26] Syringe Pump, 2016, http://www.thingiverse.com/thing:1923150 (Accessed 12 April 2017).
[27] S.J. Leigh, R.J. Bradley, C.P. Purssell, D.R. Billson, D.A. Hutchins, A simple, low-cost conductive composite material for 3D printing of electronic sensors, PLoS One 7 (2012) 1–6.
[28] I.E. Stewart, A.R. Rathmell, L. Yan, S. Ye, P.F. Flowers, W. You, et al., Solution-processed copper-nickel nanowire anodes for organic solar cells, Nanoscale 6 (2014) 5980–5988.
[29] I.E. Stewart, S. Ye, Z. Chen, P.F. Flowers, B.J. Wiley, Synthesis of Cu–Ag, Cu–Au, and Cu–Pt core–shell nanowires and their use in transparent conducting films, Chem. Mater. 27 (2015) 7788–7794.
[30] Okan Yurduseven, Patrick Flowers, Shengrong Ye, Daniel Marks, Jonah Gollub, Thomas Fromenteze, Benjamin Wiley, David Smith, Computational microwave imaging using 3D printed conductive polymer frequency-diverse metasurface antennas, Accepted manuscript Source: IET Microwaves, Antennas & Propagation, 10 pp. 10.1049/iet-map.2017.0104, Online ISSN 1751–8733,Available online: 18 September.
[31] Y. Xie, S. Ye, C. Reyes, P. Sithikong, B. Popa, B.J. Wiley, Microwave metamaterials made by fused deposition 3D printing of a highly conductive copper-based filament, Appl. Phys. Lett. 110 (2017) 181903.
[32] S. Roy, M.B. Qureshi, S. Asif, B.D. Braaten, A model for 3D-printed microstrip transmission lines using conductive electrifi filament, Accepted for Presentation at the 2017 IEEE International Symposium on Antennas and Propagation (2017) 1–2, WE-A5.1P.10.
[33] D. Spaulding, D-Bot, Thingiverse, 2015, http://www.thingiverse.com/thing:1001065 (Accessed 9 March 2017).
[34] 3D Printing Electronic Components and Circuits with Conductive Thermoplastic Filament, Thingiverse (2017). http://www.thingiverse.com/thing:2281247 (Accessed 29 April 2017).
[35] P. Scherz, S. Monk, Practical Electronics for Inventors, fourth ed., McGraw Hill Professional, 2016.
[36] H.A. Wheeler, Simple inductance formulas for radio coils, Proc. IRE 16 (1928) 1398–1400.
[37] D.S. Kalenov, V.V. Meriakri, M.P. Parkhomenko, S. Zhou, Dielectric properties of biocompatible and biodegradable polycaprolone and polylactide and their nanocomposites in the millimeter wave band, AIP Conf. Proc. 1459 (2012) 77–79.
[38] L. Anderson, M. Jacob, Microwave characterization of a novel environmentally friendly, plasma polymerized organic thin film, Phys. Procedia 14 (2011) 87–90.
[39] Y. Rao, C.P. Wong, Ultra high dielectric constant epoxy silver composite for embedded capacitor application, Electr. Compon. Technol. Conf. (2002) 920–923.
[40] F. Cohen Tenoudji, First and second order systems, in: Analog and Digital Signal Analysis, Springer International Publishing, Cham, 2016, pp. 11–34.